A Fast Endmember Estimation Algorithm from Compressive Measurements

Edwin Vargas*, Samuel Pinilla† and Henry Arguello‡
*† Department of Electronic Engineering, Universidad Industrial de Santander
‡ Department of Computer Science, Universidad Industrial de Santander
Email: *edwin.vargas4@correo.uis.edu.co, †samuel.pinilla@correo.uis.edu.co, ‡henarfu@uis.edu.co

***Abstract*—This paper deals with estimating the endmembers in a linear mixing model (LMM) of a hyperspectral image, from measurements acquired with compressive spectral imaging (CSI) devices. For this problem, a novel approach is developed exploiting the Rayleigh-Ritz (RR) theory to approximate the signal subspace where the data lie and the fact that the endmembers are located at the vertices of a simplex set under a LMM. The proposed approach first estimates a subset of eigenvectors to approximate the signal subspace using the RR theory, and then vertex component analysis is applied to find the endmembers in the approximated subspace. Simulations results conducted on realistic compressive hyperspectral images show that the proposed algorithm can provide endmembers results very close to those obtained when using uncompressed images, with the advantage of using a reduced number of measurements. In particular, the numerical tests show that the proposed approach is able to estimate the endmembers using 50% of the full data.**

I. Introduction

Hyperspectral (HS) sensors collect data that can be represented by a three-dimensional data cube [1]. This data cube, referred to as HS image, is a collection of 2D images, where each 2D image is captured at a specific wavelength. HS images are characterized by a high-spectral-resolution which allows an accurate identification of the different materials contained in the scene of interest. Analyzing the spectral information of HS images has allowed the development of many applications in the fields of remote sensing [2], medical imaging [3] and astronomy [4].

Commonly, each pixel of a HS image is assumed to be a mixture of different spectral signatures, referred to as endmembers. The procedure by which the spectral signature is decomposed into a collection of these components and a set of corresponding fractions is a highly investigated process known as spectral unmixing [5], [6]. In general, there exist two models for the mixing process, linear and nonlinear. In particular, the linear mixing model (LMM) assumes that each pixel of the target image is a linear mixture of spectral signatures. Thus, we can represent each observed spectral vector as $\mathbf{y} = \mathbf{M}\boldsymbol{\alpha}$, where $\mathbf{M} = [\mathbf{m}_1, \cdots, \mathbf{m}_p] \in \mathbb{R}^{L\times p}$ is the endmember matrix whose columns are spectral signatures, p is the number of materials contained in the image, L is the number of spectral bands, and $\boldsymbol{\alpha} = [\alpha_1, \cdots, \alpha_p]^T \in \mathbb{R}^p$ contains the abundance fractions of the endmembers [6]. Under this model, many geometrical, statistical and sparse regression approaches have been proposed to address the spectral unmixing problem (see [5] for a complete overview). Also, LMM is a well known and simple model which holds approximately when the mixing scale is macroscopic and the interaction between the reflected radiation of each endmember is negligible. Conversely, the nonlinear mixing model is a better approximation when the mixing scale is microscopic and the materials are said to be intimately mixed [7], [8].

On the other hand, HS images are limited by their relatively low spatial resolution [9]. In addition to their reduced spatial resolution, conventional spectral imaging devices have the drawback of requiring to scan a number of zones that grows linearly in proportion to the desired spatial or spectral resolution. Furthermore, HS images demand a large amount of data that must be stored and transmitted. To overcome this limitation, and motivated by the compressed sensing (CS) theory [10], several spectral imagers have been recently proposed [11], [12]. Compressive spectral imaging (CSI) techniques [11], [13], [14] exploit the fact that HS images are sparse in some basis and thus they can be efficiently acquired and reconstructed by using CS theory. As a consequence, the images acquired with CSI have a reduced number of measurements compared to those obtained with conventional spectral imaging devices, reducing, in turn, the amount of data that has to be stored and transmitted.

However, standard endmember extraction algorithms, such as VCA [15], SVMAX [16] or N-FINDR [17] cannot be directly applied when the observed images have been compressed. Additionally, the methods based on spectral unmixing and the CS theory reported in [18], [19], [20], assume that the endmembers are known a priori. In general, this assumption does not hold for many practical applications, where knowledge about endmember spectral signatures are highly incomplete, or even totally missing.

Therefore, in this work we present an algorithm dealing with endmember estimation directly from compressive measurements. More specifically, we aim at estimating the endmembers in a linear mixing scenario considering CSI systems those proposed in [12], [21]. We exploit the geometrical fact that, under the LMM, hyperspectral vectors belong to a simplex set whose vertices correspond to the endmembers, and lie in a subspace of dimension p. We also exploit the Rayleigh-Ritz theory which can be used to approximate the signal subspace from random projections [22]. More precisely, the proposed algorithm first estimates a subset of eigenvectors to approximate the signal subspace using the Rayleigh-Ritz theory, then reconstruct the spectral vector using least squares (pseudoinverse) and projects them in the subspace spanned by the eigenvectors already determined. Finally, vertex component analysis is applied to find the endmembers in the projected subspace.

The paper is organized as follows. Section II surveys relevant background surrounding the Rayleigh-Ritz theory and vertex component analysis (VCA). The observation model for the compressed measurements and the formulation problem are presented in Section III. The procedure to estimate the signal subspace is described in Section IV. Numerical results conducted on realistic compressed HS

ISBN 978-90-827970-1-5 © EURASIP 2018

images are presented in Section V, whereas conclusions are summarized in Section VI.

II. Preliminary Background

This section presents two required procedures to rapidly estimate the endmembers from compressive measurements. Specifically, we briefly introduce the Vertex Component Analysis (VCA) and the Rayleigh-Ritz (RR) procedure.

A. Vertex Component Analysis

Vertex component analysis (VCA) is a numerical tool to estimate the endmembers of a scene under a linear mixing scenario, which exploits two facts. First, the endmembers are located at the vertices of a simplex. Second, VCA uses the fact that an affine transformation of a simplex set is also a simplex set [15]. Specifically, VCA models the spectral measurements as $\mathbf{y} = \mathbf{M}\gamma\boldsymbol{\alpha}$, where γ is a scale factor modeling the illumination variability, and the fractional abundance $\boldsymbol{\alpha}_j$ represents the fractional area occupied by the $\mathbf{m}_j$ endmember. Also, this model leads to two constraints. First, the spectral signature is a nonnegative linear combination of endmemembers. Second, the abundances sum to one. Thus, the complete set of measurements $C_p = \{\mathbf{y} \in \mathbb{R}^L : \mathbf{y} = \mathbf{M}\gamma\boldsymbol{\alpha}, \boldsymbol{\alpha} \succeq 0, 1^T\boldsymbol{\alpha} = 1, \gamma \geq 0\}$ is a convex cone in $\mathbb{R}^L$. Based on this model, the VCA algorithm projects this cone onto a properly chosen hyperplane resulting in a simplex S_p with vertices being the endmembers. To find the endmembers, the algorithm works as follows (see [5][15] for more details):

1) Generate a random vector $\mathbf{f}$ orthonormal to the subspace spanned by the endmembers already determined.
2) Project the data $\mathbf{Y} = [\mathbf{y}_1, \cdots, \mathbf{y}_N]$, with N as the number of pixels, onto $\mathbf{f}$, i.e. $\mathbf{v} = \mathbf{Y}^T\mathbf{f}$.
3) Find the endmember $\mathbf{y}_k$ that maximizes the projection, where $k := \arg\max_{j=1,\cdots,N} |\mathbf{v}|$.
4) Repeat until all endmembers are exhausted.

B. Rayleigh-Ritz procedure

The Rayleigh-Ritz procedure is a method for finding approximations to eigenvalues and eigenvectors of a given matrix $\mathbf{A} \in \mathbb{R}^{n\times n}$ that cannot be solved analytically [22]. The procedure is as follows

1) Compute an orthonormal basis $\mathbf{B} \in \mathbb{R}^{n\times m}$, with $m \leq n$, approximating the eigenspace corresponding to m eigenvectors.
2) Compute $\mathbf{R} = \mathbf{B}^T\mathbf{A}\mathbf{B}$.
3) Compute the eigenvalues of $\mathbf{R}$ solving $\mathbf{R}\mathbf{r}_i = \tilde{\lambda}_i\mathbf{r}_i$.
4) Form the Ritz pairs $(\tilde{\lambda}_i, \mathbf{u}_i) = (\tilde{\lambda}_i, \mathbf{R}\mathbf{r}_i)$, $i = 1, \cdots, m$.

Estimated Ritz pairs are the best approximations to the pairs $(\lambda_i, \mathbf{w}_i)$ for $i = 1, \cdots, m$, where λ_i and $\mathbf{w}_i$ are the eigenvalues and eigenvectors of the matrix $\mathbf{A}$, respectively. Further, the following theorem establishes how close are the m calculated Ritz pairs to $(\lambda_i, \mathbf{w}_i)$ for $i = 1, \cdots, m$.

Theorem II.1. *Consider that the matrix $\mathbf{A}$ has spectrum $\mathcal{S}_\mathbf{A} = \{\lambda_1(\mathbf{A}), \cdots, \lambda_N(\mathbf{A})\}$, where the eigenvalues satisfy $\lambda_1(\mathbf{A}) \geq \lambda_2(\mathbf{A}) \geq \cdots \geq \lambda_N(\mathbf{A})$. The corresponding unit eigenvectors are $\mathbf{w}_i$, for all $i = 1, \cdots, N$. Suppose that, for a given Ritz vector $\mathbf{u}_{k_0}$ the eigenpair $(\lambda_{k_0}(\mathbf{A}), \mathbf{w}_{k_0})$ satisfies that*

$$\lambda_{k_0}(\mathbf{A}) = \arg\min_{\lambda\in\mathcal{S}_\mathbf{A}} |\lambda - \rho(\mathbf{u}_{k_0})|, \tag{1}$$

where $\rho(\mathbf{u_k}) = \mathbf{u}_k^T\mathbf{A}\mathbf{u}_k$. Then,

$$|\sin(\phi_{k_0})| \leq \frac{\|\mathbf{A}\mathbf{u}_{k_0} - \mathbf{u}_{k_0}\rho(\mathbf{u}_{k_0})\|_2}{\gamma_{k_0}}, \tag{2}$$

where θ_{k_0} is the angle between $\mathbf{u}_{k_0}$ and $\mathbf{w}_{k_0}$, with

$$\gamma_{k_0} = \min_{\lambda\in\mathcal{S}_\mathbf{A}, \lambda\neq\lambda_{k_0}(\mathbf{A})} |\lambda - \rho(\mathbf{u}_{k_0})|. \tag{3}$$

Proof: The proof of this theorem can be found in [22]. ■

Notice that, from Theorem II.1, the Ritz pairs $(\tilde{\lambda}_i, \mathbf{u}_i)$ can be considered a reasonable approximation to m eigenpairs $(\lambda_i(\mathbf{A}), \mathbf{w}_i)$, as it can be seen in (2).

III. Problem formulation

In this section we introduce the observation model of CSI systems and an orthogonal formulation in order to include the Rayleigh-Ritz procedure in the context of CSI acquisition model.

A. Observation model

We consider the following model for the observed compressive hyperspectral image

$$\mathbf{Y} = \mathbf{H}\mathbf{X} \tag{4}$$

where $\mathbf{X} \in \mathbb{R}^{L\times N}$ is the hyperspectral image, with L as the number of spectral bands and N as the number of pixels; $\mathbf{H} \in \mathbb{R}^{M\times L}$ models the sensing process; and $\mathbf{Y} \in \mathbb{R}^{M\times N}$ represents the acquired data, where M is the number of measurements. In a CS scenario, it is assumed that $M \ll L$. In (4) we consider that $\mathbf{X} = [\mathbf{x}_1, \cdots, \mathbf{x}_N]$, where each column $\mathbf{x}_i$ is the spectral signature of a pixel of the hyperspectral image.

B. Compressive Orthogonal Random Projections

Based on the acquisition model introduced in (4), and taking into account the singular value decomposition (SVD) of the matrix $\mathbf{H}$, one can obtain that

$$\mathbf{Y} = (\mathbf{U}\mathbf{D}\mathbf{V}^T)\mathbf{X}, \tag{5}$$

where $\mathbf{H} = \mathbf{U}\mathbf{D}\mathbf{V}^T$, $\mathbf{U} \in \mathbb{R}^{M\times M}$, $\mathbf{V} \in \mathbb{R}^{L\times L}$ satisfy that $\mathbf{U}^T\mathbf{U} = \mathbf{I}_M$, $\mathbf{V}\mathbf{V}^T = \mathbf{I}_L$, and $\mathbf{D} \in \mathbb{R}^{M\times L}$ is a diagonal matrix. Note that, given that $M \ll L$, the matrix $\mathbf{H}$ is rank deficient, which implies that the inverse problem concerning to estimate $\mathbf{X}$ is an ill-posed problem [23]. Thus, in order to solve this limitation we first estimate the closest full column rank approximation to the matrix $\mathbf{H}$. Specifically, we consider the following lemma for calculating the full column rank approximation of the matrix $\mathbf{H}$.

Lemma III.1. *Define $r = rank(\mathbf{H})$, with $r \leq M$. Then, the best low rank approximation of the matrix $\mathbf{H}$ is the following truncated matrix*

$$\tilde{\mathbf{H}} = \tilde{\mathbf{U}}\tilde{\mathbf{D}}\tilde{\mathbf{V}}^T, \tag{6}$$

where $\tilde{\mathbf{U}} \in \mathbb{R}^{M\times r}$ is the matrix $\mathbf{U}$ in (5) with the last $M-r$ columns removed, $\tilde{\mathbf{V}} \in \mathbb{R}^{L\times r}$ is the matrix $\mathbf{V}$ in (5) with the last $(L-r)$ columns removed, and $\tilde{\mathbf{D}} \in \mathbb{R}^{r\times r}$ is a diagonal matrix, where its entries are given by the first r entries in the main diagonal of $\mathbf{D}$ in (5).

Proof: The proof of this lemma is developed in [24]. ■

ISBN 978-90-827970-1-5 © EURASIP 2018

Considering the full column rank closest approximation established in Lemma III.1, we can equivalently approximate the measurements in (4) as

$$\tilde{\mathbf{Y}} = \tilde{\mathbf{D}}\mathbf{U}^T\mathbf{Y} = \tilde{\mathbf{V}}^T\mathbf{X}, \tag{7}$$

The main motivation for considering this approximated system in (7) is that this provides a link between the Rayleigh-Ritz theory and CSI model. Considering the system (7), it can be observed that

$$\tilde{\mathbf{Y}}\tilde{\mathbf{Y}}^T/N = \tilde{\mathbf{V}}^T\mathbf{X}\mathbf{X}^T\tilde{\mathbf{V}}/N = \tilde{\mathbf{V}}^T\mathbf{\Sigma}\tilde{\mathbf{V}}, \tag{8}$$

where $\mathbf{\Sigma}$ represents the covariance matrix of the dataset $\mathbf{X}$. Further, notice that $\mathbf{X}\mathbf{X}^T = \mathbf{\Sigma}$ is valid when the dataset has zero mean. Moreover, it is worth nothing that taking $\mathbf{A} = \mathbf{\Sigma}$, and $\mathbf{B} = \tilde{\mathbf{V}}$, the matrix $\tilde{\mathbf{Y}}\tilde{\mathbf{Y}}^T/N$ in (8) represents the matrix $\mathbf{R}$ in the Rayleigh-Ritz procedure summarized in Section II-B. Further, according to Theorem II.1, the eigenvectors of $\mathbf{\Sigma}$, which are the basis of the subspace in which the dataset $\mathbf{X}$ lies, can be approximated using the pairs $(\tilde{\lambda}_i, \mathbf{u}_i)$ yielded by the Rayleigh-Ritz procedure. The next section introduces a recent technique based on Principal Component Analysis (PCA) to estimate eigenvectors of the covariance matrix $\mathbf{\Sigma}$ using the Ritz vectors.

IV. Signal Subspace Estimation

This section presents a procedure to estimate the finite dimensional space in which the sensed hyperspectral image $\mathbf{X}$ belongs. In fact, in order to take advantage of the statistical relationship between the covariance matrix of the data $\mathbf{\Sigma}$ and the measurements in (8), we use the Compressive-Projection Principal Component Analysis (CPPCA) technique developed in [25] to estimate the eigenvectors from compressive measurements explained as follows.

A. CPPCA procedure

First, we aim at estimating the eigendecomposition of the covariance matrix $\mathbf{\Sigma}$ from the approximated measurements $\tilde{\mathbf{Y}}$ in (7). To do that, first consider the covariance matrix $\mathbf{\Sigma} = \mathbf{W}\mathbf{\Lambda}\mathbf{W}^T$ such that $\mathbf{W} = [\mathbf{w}_1, \cdots, \mathbf{w}_L]$, and $\mathbf{w}_i$, for $i = 1, \cdots, N$ are the unit eigenvectors. Then, consider a fixed eigenvector $\mathbf{w}_k$. Given the fact that matrix $\tilde{\mathbf{V}}$ is orthogonal, then the orthogonal projector to the generated subspace $\mathcal{P}$ by the matrix $\tilde{\mathbf{V}}$ is given by $\tilde{\mathbf{V}}\tilde{\mathbf{V}}^T$ [22]. Thus, the normalized orthogonal projection of $\mathbf{w}_k$ onto $\mathcal{P}$ is given by

$$\mathbf{v}_k = \frac{\tilde{\mathbf{V}}\tilde{\mathbf{V}}^T\mathbf{w}_k}{\|\tilde{\mathbf{V}}\tilde{\mathbf{V}}^T\mathbf{w}_k\|_2}. \tag{9}$$

Then, considering (9), in the CPPCA approach is observed that building an auxiliary subspace $\mathcal{Q}$ given by

$$\mathcal{Q}_k = \mathcal{P}^{\perp} \oplus \text{span}(\mathbf{v}_k), \tag{10}$$

contains the eigenvector $\mathbf{w}_k$ [25], $i.e.$ $\mathbf{w}_k \in \mathcal{Q}_k$, where $\mathcal{P}^{\perp}$ denotes the orthogonal complement of $\mathcal{P}$. Moreover, according to the sensing process in (7) we can split the dataset $\mathbf{X} = [\mathbf{x}_1, \mathbf{x}_2, \cdots, \mathbf{x}_N]$ into J partitions $\mathbf{X}^{(j)}$ each one associated with its own randomly chosen projection $\tilde{\mathbf{V}}^{(j)}$, for $j = 1, \cdots, J$. We assume that the dataset is separated such that each $\mathbf{X}^{(j)}$ closely resembles the whole dataset $\mathbf{X}$ statistically and so it has approximately the same eigendecomposition [26], [27]. Thus, forming the corresponding subspaces $\mathcal{Q}_k^{(j)}$ for each partition (j) via (10) it can be concluded that $\mathbf{w}_k \in \mathcal{Q}_k^{(1)} \cap \cdots \cap \mathcal{Q}_k^{(J)}$. Since we do not have knowledge about the normalized projections $\mathbf{v}_k^{(j)}$, under the assumption that eigenvalue $\lambda_k(\mathbf{\Sigma})$ is sufficiently separated in value with respect to the other ones, we can use the Ritz vectors $\mathbf{u}_k^{(j)}$ to approximate $\mathbf{v}_k^{(j)}$ and form the spaces $\mathcal{Q}_k^{(j)}$ [25]. Considering these conditions and due to $\mathcal{Q}_k^{(j)}$ are convex and closed, a projection onto convex set optimization can be used to approximate $\mathbf{W}$. Thus, iteratively the eigenvector $\mathbf{w}_k$ can be approximated as

$$\hat{\mathbf{w}}_k^{(i)} = \frac{1}{J}\sum_{j=1}^{J} \mathbf{Q}_k^{(j)}\mathbf{Q}_k^{(j)^T}\hat{\mathbf{w}}_k^{(i-1)}, \tag{11}$$

where i is the iteration index, the projection onto $\mathcal{Q}^{(j)}$ is performed by the matrix $\mathbf{Q}_k^{(j)} = \left[\mathbf{u}_k^{(j)}, \mathbf{I} - \tilde{\mathbf{V}}^{(j)}\tilde{\mathbf{V}}^{(j)T}\right] \in \mathbb{R}^{L\times(L+1)}$, and CPPCA initializes $\hat{\mathbf{w}}_k^{(0)}$ to the average of the Ritz vectors [25]. The iterations in (11) converges to $\hat{\mathbf{w}}_k$ which after appropriate normalization will approximate the desired eigenvector $\mathbf{w}_k$ (up to sign) [25]. Finally, we note that a limitation of CPPCA is given by the fact that the Rayleigh-Ritz method requires well separated eigenvalues, which in HS images is true for the first largest eigenvalues.

B. Partitions in a real CSI system

In an ideal CSI system where we can obtain a non-restricted coding, we can split the dataset $\mathbf{X}$ in many ways. However, in real CSI systems, where we have approximations to the ideal case, the splitting of the dataset $\mathbf{X}$ in the previous procedure are restricted by the sensing architecture. For simulations we choose the optical Spatio Spectral Encoded Compressive HS imager (SSCSI) proposed in [21], where the spatio-spectral modulation is achieved by applying a diffraction grating to disperse the light into spectrum and inserting a coded attenuation mask between the spectrum plane and the sensor plane. Thus, the coded sensor image is measured by multiplying each spectral band with modulation matrices that have the same coded but sheared by a different amount [21]. This correlation between bands make the number of partitions be at most $J = L$. For simulations we set $J = L$ and we assume that these partitions share the statistical properties of the complete dataset.

C. Endmember Estimation Algorithm

This section presents the proposed algorithm for estimating the endmembers from compressive measurements. Algorithm 1 summarizes the proposed procedure.

Algorithm 1 Endmember Estimation Algorithm

1: **Input:** $\mathbf{Y} \in \mathbb{R}^{M\times N}$, $\mathbf{H} \in \mathbb{R}^{M\times L}$. Choose the number of partitions J.
2: $\tilde{\mathbf{H}} = \tilde{\mathbf{U}}\tilde{\mathbf{D}}\tilde{\mathbf{V}}^T$ ▷ (5)
3: $\tilde{\mathbf{Y}} = \tilde{\mathbf{V}}^T\mathbf{X}$ ▷ (7)
4: $\hat{\mathbf{W}} \leftarrow \text{CPPCA}(\tilde{\mathbf{Y}}, \tilde{\mathbf{V}}, J)$ ▷ Algorithm 2
5: $\hat{\mathbf{M}} \leftarrow \text{VCA}(\hat{\mathbf{W}}_d, \tilde{\mathbf{Y}})$ ▷ Algorithm in [15]
6: **Return** $\hat{\mathbf{M}}$

First, Algorithm 1 estimates the measurements of the CSI system using the approximation defined in (7). Second, the basis of the signal subspace ($i.e.$ $\hat{\mathbf{W}}_d$) is estimated from the first d columns of $\hat{\mathbf{W}}$ using the CPPCA procedure. For the sake of completeness of the proposed approach, CPPCA procedure is described in Algorithm 2. CPPCA computes

ISBN 978-90-827970-1-5 © EURASIP 2018

the corresponding PCA coefficients using the pseudoinverse $\mathbf{Z}^{(j)} = (\tilde{\mathbf{V}}^{(j)T}\mathbf{W}_d)^{+}\tilde{\mathbf{Y}}^{(j)}$. Finally, the VCA procedure is performed to the subspace previously identified. Here, we note that if we project the cone C_p, which lie in a subspace of dimension p in a subspace $E_d \supset E_p$, followed by a projection in a properly hyperplane, the projection is still a simplex with the same vertices that S_p.

Algorithm 2 CPPCA Procedure [25]

procedure CPPCA($\tilde{\mathbf{Y}}, \tilde{\mathbf{V}}, J$) ▷ CPPCA procedure
  Determine $\left\{\tilde{\mathbf{V}}^{(1)}, \cdots, \tilde{\mathbf{V}}^{(J)}\right\}$
  Set: $\left\{\tilde{\mathbf{Y}}^{(j)} = \tilde{\mathbf{V}}^{(j)^T}\mathbf{X}^{(j)} | \quad j = 1, \cdots, J\right\}$
  Estimate the Ritz vectors $\left\{\mathbf{u}_k^{(j)} | \quad k = 1, \cdots, L, \ j = 1, \cdots, J\right\}$ of the L eigenvectors $\mathbf{w}_k$ of the matrix $\tilde{\mathbf{\Sigma}}^{(j)}$, according to Section II-B. ▷ (8)
  $\mathbf{P}^{(j)^\perp} = \mathbf{I} - \tilde{\mathbf{V}}^{(j)}\tilde{\mathbf{V}}^{(j)^T}$
  for $k = 1 : L$ **do**
    $\mathbf{Q}_k^{(j)} = \left[\mathbf{u}_k^{(j)}, \mathbf{P}^{(j)^\perp}\right]$ ▷ (10)
    $\hat{\mathbf{w}}_k^{(0)} = \frac{1}{JL}\sum_{k,j}\mathbf{u}_k^{(j)}$.
    for $i = 1 : T$ **do**
      $\hat{\mathbf{w}}_k^{(i)} = \frac{1}{J}\sum_{j=1}^{J}\mathbf{Q}_k^{(j)}\mathbf{Q}_k^{(j)^T}\hat{\mathbf{w}}_k^{(i-1)}$ ▷ (11)
    end for
  end for
  Return $\hat{\mathbf{W}} = [\hat{\mathbf{w}}_1, \cdots, \hat{\mathbf{w}}_L]$
end procedure

V. Experimental Results

In this section, we examine the performance of the proposed method and we choose the VCA algorithm, which does not use compressive measurements, for comparison. Two real-world data sets were considered: Urban and Jasper [28]. The observed measurement were generated by compressing the hyperspectral images with a sensing matrix whose entries were drawn using a Bernoulli distribution. This sensing matrix models the coded aperture in the considered CSI device (SSCSI), where the value "1" of the Bernoulli variable corresponds to a light transmissive element and the value "0" to a blocking element. Additionally, the measurements were contaminated by additive Gaussian noise, with SNR=25 dB. For both datasets, the number of projections is $K = 0.5L$ leading to a compression ratio (K/L) of 50%. The number of partitions is $J = L$ as discussed above. Finally, the quality of the estimated endmembers is evaluated using the normalized mean square error of the endmember matrix (NMSE_M) and the averaged spectral angle mapper (SAM) to measure the spectral distortion.

A. Urban Data Set

In this experiment the reference image is the Urban data set generated by the Hyperspectral Digital Imagery Collection Experiment (HYDICE) on an urban area. We only worked in a section of 128×128 pixels and we remove low SNR and water-vapor absorption bands resulting in a HS reference image of size $128 \times 128 \times 162$. The number of endmembers present in Urban are $p = 6$, including roof, grass, asphalt, tree, metal and dirt. The estimated endmembers are displayed in Fig. 1 whereas quantitative results are provided in Table I.

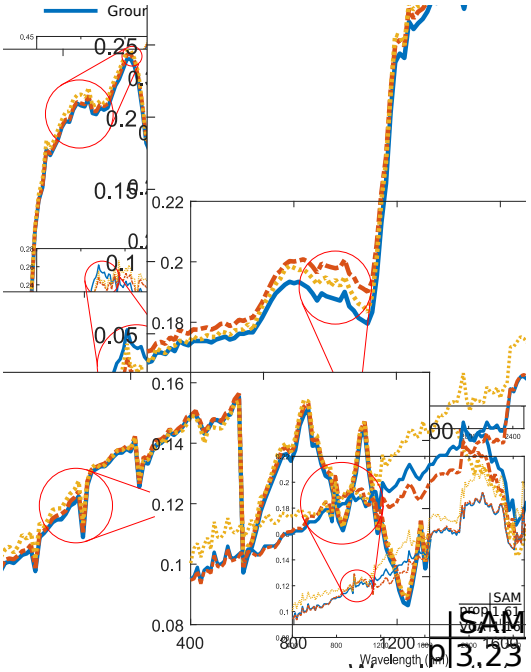

Fig. 1: Six unmixed endmembers for the Jasper dataset obtained using VCA (on full data) and the proposed method (on 50% of measurements) and compared with the ground truth.

TABLE I: Unmixing Performance (Urban data set): SAM (degrees), NMSE_M (in Decibels), Time (seconds) and the amount of data (%)

Methods	SAM_M	NMSE_M	Time	Data
Proposed	1.6388	-28.3270	1.42	**50%**
VCA	**1.3758**	**-30.9109**	**0.19**	100%

B. Jasper Data set

In this experiment the reference image is the Jasper Ridge image collected by the Airbone Visible/Infrared Imaging Spectrometer (AVIRIS) over Jasper Ridge in central California, USA. We only worked in a section of 128×128 pixels and we remove low SNR and water-vapor absorption bands resulting in a HS reference image of size $128 \times 128 \times 198$. The number of endmembers present in Jasper is $p = 4$, including soil, water, tree, and road. The estimated endmembers are shown in Fig. 2 whereas quantitative results are provided in Table II.

TABLE II: Unmixing Performance (Jasper data set): SAM (degrees), NMSE_M (Decibels), Time (seconds) and amount of data (%)

Methods	SAM_M	NMSE_M	Time	Data
Proposed	2.2052	-35.9368	1.37	**50%**
VCA	**1.4804**	**-39.7149**	**0.18**	100%

C. Discussion

As can be observed in Fig. 1 and 2, the recovered endmembers, using the proposed algorithm on 50% of measurements, exhibit close representations with respect to those belonging to the ground truth. Furthermore, as can be seen in the details in Fig. 1 and 2, the estimated endmembers using the proposed approach can follow complex changes of the endmember signature. Finally, the SAM values in Fig.

ISBN 978-90-827970-1-5 © EURASIP 2018

1 and 2 indicate that the proposed approach (on 50% of measurements) has a competitive performance compared to that obtained with the VCA procedure on full dataset.

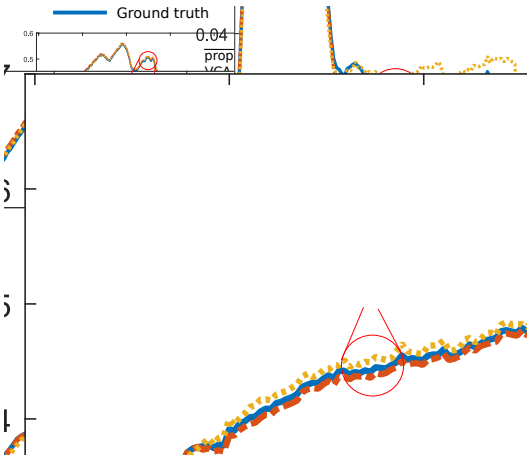

Fig. 2: Four unmixed endmembers for the Jasper dataset obtained using VCA (on full data) and the proposed method (on 50% of measurements) and compared with the ground truth.

On the other hand, the numerical results in Table I and II show that the proposed approach is able to estimate the endmembers from compressive measurements. Also, it is important to remark that our method exhibits a similar performance to estimate the endmembers compared with VCA, using less amount of data. We finally note that the proposed method spends more time due to the signal subspace estimation. However, this is a fast approach when compressive HS images are considered.

VI. Conclusions

This paper presented a new algorithm to estimate the endmembers of an hyperspectral image in a linear mixing scenario directly from compressive measurements. Our results showed that it is possible to recover the endmembers from compressive measurements in a rational time and these are very close to the endmembers extracted using a full hyperspectral image. Future work includes the estimation of the number of endmembers directly from the compressive measurements. Due to the limitations of CPPCA to estimate the signal subspace, other methods for this estimation will be relevant for further research.

References

[1] S. May and H. Burke, "Multisensor Fusion with Hyperspectral Imaging Data: Detection and Classification," *Lincoln Laboratory Journal*, vol. 14, no. 1, 2003.

[2] M. Schaepman, S. Ustin, A. Plaza, T. Painter, J. Verrelst, and S. Liang, "Earth system science related imaging spectroscopy-An assessment," *Remote Sens. Environ.*, vol. 113, no. 123–137, 2009.

[3] S. Panasyuk, S. Yang, D. Faller, D. Ngo, R. Lew, J. Freeman, and A. Rogers, "Medical hyperspectral imaging to facilitate residual tumor identification during surgery," *Cancer biology & therapy*, vol. 6, no. 3, pp. 439–446, 2007.

[4] K. Hege, D. O'Connell, W. Johnson, S. Basty, and E. Dereniak, "Hyperspectral imaging for astronomy and space surviellance," in *Optical Science and Technology, SPIE's 48th Annual Meeting*, 2004, pp. 380–391.

[5] J. Bioucas, A. Plaza, N. Dobigeon, M. Parente, Q. Du, P. Gader, and J. Chanussot, "Hyperspectral unmixing overview: Geometrical, statistical, and sparse regression-based approaches," *IEEE J. Sel. Top. Appl. Earth Obs. Remote Sens.*, vol. 5, no. 2, pp. 354–379, 2012.

[6] N. Keshava and J. Mustard, "Spectral unmixing," *IEEE Signal Process. Mag.*, vol. 19, no. 1, pp. 44–57, 2002.

[7] Y. Altmann, N. Dobigeon, S. McLaughlin, and J.-Y. Tourneret, "Nonlinear spectral unmixing of hyperspectral images using gaussian processes," *IEEE Trans. Signal Process.*, vol. 61, no. 10, pp. 2442–2453, 2013.

[8] R. Heylen, D. Burazerovic, and P. Scheunders, "Non-linear spectral unmixing by geodesic simplex volume maximization," *IEEE J. Sel. Topics Signal Process.*, vol. 5, no. 3, pp. 534–542, 2011.

[9] G. Shaw and H. Burke, "Spectral imaging for remote sensing," *Lincoln Laboratory Journal*, vol. 14, no. 1, pp. 3–28, 2003.

[10] D. Donoho, "Compressed sensing," *IEEE Trans. inf. Theory*, vol. 52, no. 4, pp. 1289–1306, 2006.

[11] M. Gehm, R. John, D. Brady, R. Willett, and T. Schulz, "Single-shot compressive spectral imaging with a dual-disperser architecture," *Optics express*, vol. 15, no. 21, pp. 14 013–14 027, 2007.

[12] C. Correa, H. Arguello, and G. Arce, "Snapshot colored compressive spectral imager," *JOSA A*, vol. 32, no. 10, pp. 1754–1763, 2015.

[13] G. Arce, D. Brady, L. Carin, H. Arguello, and D. Kittle, "Compressive coded aperture spectral imaging: An introduction," *IEEE Signal Process. Mag.*, vol. 31, no. 1, pp. 105–115, 2014.

[14] H. Arguello and G. Arce, "Spectrally Selective Compressive Imaging by Matrix System Analysis," in *Imaging Appl. Opt. Tech. Pap.* Washington, D.C.: OSA, jun 2012, p. CM4B.5.

[15] J. Nascimento and J. Dias, "Vertex component analysis: A fast algorithm to unmix hyperspectral data," *IEEE Trans. Geosci. Remote Sens.*, vol. 43, no. 4, pp. 898–910, 2005.

[16] T.-H. Chan, W.-K. Ma, A. Ambikapathi, and C.-Y. Chi, "A simplex volume maximization framework for hyperspectral endmember extraction," *IEEE Trans. Geosci. Remote Sens.*, vol. 49, no. 11, pp. 4177–4193, 2011.

[17] M. Winter, "N-FINDR: An algorithm for fast autonomous spectral end-member determination in hyperspectral data," in *SPIE's International Symposium on Optical Science, Engineering, and Instrumentation*, Denver, CO, USA, 1999, pp. 266–275.

[18] J. Liu and J. Zhang, "Spectral unmixing via compressive sensing," *IEEE Trans. Geosci. Remote Sens.*, vol. 52, no. 11, pp. 7099–7110, 2014.

[19] C. Li, T. Sun, K. Kelly, and Y. Zhang, "A compressive sensing and unmixing scheme for hyperspectral data processing," *IEEE Trans. Image Process.*, vol. 21, no. 3, pp. 1200–1210, 2012.

[20] A. Ramirez, G. Arce, and B. Sadler, "Spectral image unmixing from optimal coded-aperture compressive measurements," *IEEE Trans. Geosci. Remote Sens.*, vol. 53, no. 1, pp. 405–415, 2015.

[21] X. Lin, Y. Liu, J. Wu, and Q. Dai, "Spatial-spectral encoded compressive hyperspectral imaging," *ACM Transactions on Graphics (TOG)*, vol. 33, no. 6, p. 233, 2014.

[22] B. N. Parlett, *The symmetric eigenvalue problem*. SIAM, 1998, vol. 20.

[23] K. Ito and B. Jin, *Inverse problems: Tikhonov theory and algorithms*. World Scientific, 2015.

[24] G. H. Golub, A. Hoffman, and G. W. Stewart, "A generalization of the eckart-young-mirsky matrix approximation theorem," *Linear Algebra and its applications*, vol. 88, pp. 317–327, 1987.

[25] J. Fowler, "Compressive-projection principal component analysis," *IEEE Trans. Image Process.*, vol. 18, no. 10, pp. 2230–2242, 2009.

[26] B. Penna, T. Tillo, E. Magli, and G. Olmo, "A new low complexity klt for lossy hyperspectral data compression," in *Geoscience and Remote Sensing Symposium, 2006. IGARSS 2006. IEEE International Conference on*. IEEE, 2006, pp. 3525–3528.

[27] Q. Du and J. E. Fowler, "Low-complexity principal component analysis for hyperspectral image compression," *The International Journal of High Performance Computing Applications*, vol. 22, no. 4, pp. 438–448, 2008.

[28] F. Zhu, Y. Wang, B. Fan, G. Meng, S. Xiang, and C. Pan, "Spectral unmixing via data-guided sparsity," *IEEE Trans. Image Process.*, vol. abs/1403.3155, 2014.

ISBN 978-90-827970-1-5 © EURASIP 2018